Symmetry-Breaking Assisted Landau-Zener Transitions in Rydberg Atoms

S. S. Zhang,[1,2] W. Gao,[1,2] H. Cheng,[1,2] L. You,[3,4] and H. P. Liu[1,2,*]
[1]State Key Laboratory of Magnetic Resonance and Atomic and Molecular Physics, Wuhan Institute of Physics and Mathematics, Chinese Academy of Sciences, Wuhan 430071, People's Republic of China
[2]University of Chinese Academy of Sciences, Beijing 100049, People's Republic of China
[3]State Key Laboratory of Low Dimensional Quantum Physics, Department of Physics, Tsinghua University, Beijing 100084, People's Republic of China
[4]Collaborative Innovation Center of Quantum Matter, Beijing 100084, China

(Received 21 November 2016; revised manuscript received 12 May 2017; published 8 February 2018)

We report the observation of a controlled Landau-Zener transition (LZT) in Rydberg atoms by breaking the symmetry of the underlying Hamiltonian. For a nonhydrogenic Rydberg atom inside a changing electric (F) field, a LZT occurs between the avoided crossing energy levels of neighboring Rydberg states only for a sufficiently high changing rate. If a transverse magnetic (B) field is applied as we implement, the atomic level symmetry is broken, which causes the Stark manifolds denoted by a different $|m|$ (m is the magnetic quantum number) to interact with each other. The mixed state levels end up pushing the adiabatically repelled target states closer and additionally they serve as stepping stones for the sequential LZTs between the neighboring sublevels. Such a feature significantly decreases the changing rate required for an efficient LZT inside a pure electric field. We report experimental observations that support the above scenario. It opens a versatile approach for engineering a controlled LZT in more general systems.

DOI: 10.1103/PhysRevLett.120.063203

Nonadiabatic dynamics is a paradigm in many physical systems [1–11] such as coherent beam splitting for electron spin states [8,10], the controlled driving of a superconducting qubit [4,9,12], and efficient spin transporting in a semiconductor quantum well [11]. A ubiquitous feature of such dynamics concerns the universal physics associated with the Landau-Zener transition (LZT) [13], which quantitatively describes the nonadiabatic transition rates from sweeping through an avoided crossing as illustrated in Fig. 1(a). Assuming the diabatic energy levels cross each other linearly in time, the LZT rate between the two adiabatic states is approximately given by [13]

$$p = \exp\left(-\frac{\pi\Delta^2}{2|\nu_2 - \nu_1|}\right), \tag{1}$$

where Δ is the gap minimum between the two avoided crossing levels, and ν_j denotes the "speed" along the asymptotic diabatic energy level $E_j = \nu_j(t - t_0)$ for $j = 1$ and 2, following the convention of the Planck constant $\hbar = 1$. Given a Δ, the magnitude of ν_j fully determines the LZT transition rate, and thus the associated quantum dynamic process [1,4,5]. For example, assuming a small Δ due to a weak interaction ($\sim$10 kHz), the transfer dynamics is efficiently tunable even for a slowly varying coupling in a time scale up to 200 μs [1], while for a larger gap, a faster sweeping rate is required to observe a LZT.

This Letter proposes a scenario for an enhanced LZT in a two-level system by breaking the level degeneracy, or the symmetry of the underlying Hamiltonian, as depicted in Fig. 1(b). The split of the otherwise degenerate states and the resulting sublevels push the target states closer and serve as stepping stones for significantly enhanced sequential LZTs. The underlying mechanism differs from the earlier method of simply changing the varying or sweeping rate [1,11,14].

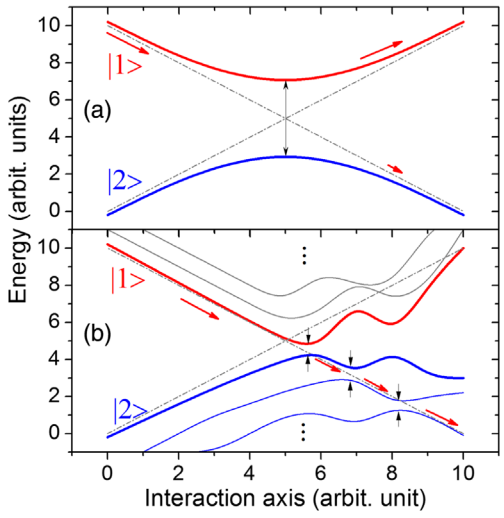

FIG. 1. A LZT over a simple two-level crossing as in (a) can be significantly enhanced with the removal of level degeneracy as in (b) due to symmetry breaking.

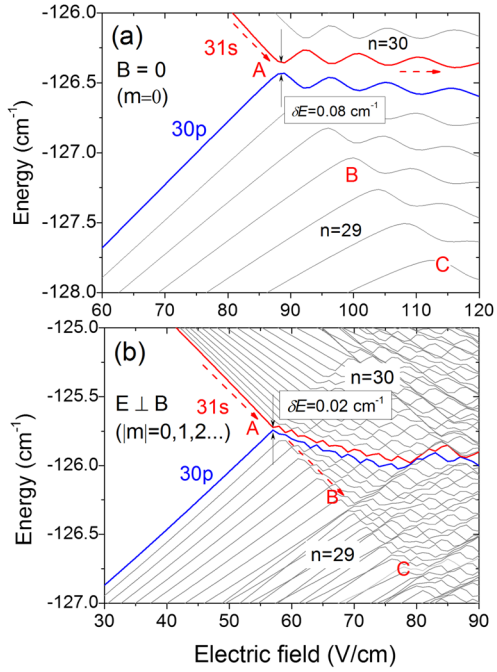

FIG. 2. Energy levels of a sodium atom inside a pure electric field exhibiting how a large energy gap (a) gets split if a crossed magnetic field is applied (b). A symmetry breaking introduced by the transverse magnetic field ($B = 0.8$ T) makes an efficient LZT that cannot occur in a pure electric field as denoted by the red dashed arrows. See the Supplemental Material [23] for the details of the map calculation with the aid of a B-spline basis [24].

This scenario is demonstrated with a Na Rydberg atom around $n = 30$ by single-photon excitation. Figure 2(a) illustrates the Stark map for a Rydberg sodium atom at $|m| = 0$ due to a single-photon π excitation from the ground state. Rich avoided crossings from core polarization [15,16] are easily noticeable. Treated as an approximate hydrogenic atom, for every $|m|$ of a given manifold n, an interaction subspace is spanned by the quantum number k running from $-(n - |m| - 1)$ to $(n - |m| - 1)$ in steps of 2. Subspaces with different $|m|$ do not couple to each other [17]. For nonhydrogen atoms like sodium (for $m = 0$), avoided crossings arise, the first of which at the weakest electric field with the minimum gap occurring at the Inglis-Teller limit [18], labeled by point A in Fig. 2(a). While below the limit, the $30p$ and $31s$ states, which are defined as the states adiabatically connected to the zero-field $30p$ and $31s$ ones, labeled in thick blue and red lines, exhibit opposite slopes, respectively. They possess induced electric dipole moments (IEDMs) of opposite signs [19]. Given the large Δ for this avoided crossing, the observation of an efficient LZT requires a large sweeping rate on the order of 10^5 V/cm μs [14,20–22].

Gaps for subsequent avoided crossings at higher electric fields, for instance, at points B and C, are increasingly larger, thus preventing efficient LZTs from occurring [25]. An atom adiabatically staying in a given Stark state, e.g., the $31s$ state, carries IEDMs of opposite signs before and after an avoided crossing. Such a feature is generic for nonhydrogen atoms at low $|m|$ states.

When a transverse B field is introduced to the nonhydrogenic Rydberg atom in a pure electric field F, however, the above discussed degeneracies are broken and the Stark manifold splits further into a more complicated level diagram that can be described by the following Hamiltonian [26–28]

$$H = \frac{p^2}{2} + V_c(r) + Fr\cos\theta + \frac{1}{2}BL_x + \frac{1}{8}B^2r^2\sin^2\theta\cos^2\phi, \quad (2)$$

in atomic units, assuming a fixed atomic core and with orthogonal F and B fields, respectively, along the z and x axes. The first three terms on the rhs of Eq. (2) are the kinetic energy, the Coulomb potential modified by the core polarization, and the Stark effect, which constitute the Hamiltonian of an atom in a pure electric field F. The terms on the second line denote the paramagnetic interaction and the diamagnetic interaction, respectively.

The symmetry breaking by the transverse B field gives rise to many sublevels and noticeable level deformations as shown in Fig. 2(b), where the magnetic field is set to $B = 0.8$ T. Unlike in a pure electric field, $|m|$ is no longer a good quantum number now and the subspaces of the Stark manifold denoted by different $|m|$ are coupled to each other by the paramagnetic term satisfying $\Delta l = \pm 1$ and $\Delta m = \pm 1$, and weakly by the diamagnetic term according to $\Delta l = 0, \pm 2$ and $\Delta m = 0, \pm 2$ [28,29]. These coupling schemes extend to all $|m|$ states. In a strong transverse B field, the large $|m|$ states repel the low $|m|$ states strongly, therefore pushing the blue state $30p$ and red state $31s$ closer, a specific example of what we discussed.

Compared to the case of a pure F field, the crossed field level diagram exhibits two distinct features that give rise to an enhanced LZT and a larger net IEDM. First, the symmetry breaking causes more states to participate in a level interaction, which reduces the overall gap and pulls the target state energy levels closer. As a result, the Inglis-Teller crossing point occurs earlier, e.g., at a lower F field, as denoted in Fig. 2(b), and the gap reduces to $\sim$0.02 cm^{-1} from $\sim$0.08 cm^{-1} in a pure electric field as shown in Fig. 2(a). Second, the level splitting gives rise to more sublevels, which reduces the gaps between the adjacent ones. For example, the gaps at subsequently higher crossing points B and C become increasingly smaller, leading to increasingly enhanced LZTs at similar sweeping rates. A larger portion of the atoms initially in the red state remains in the same sloped levels along the dashed arrows shown in Fig. 2(b). The initially prepared $31s$ ($30p$) state atoms thus can stay in the red (blue) state longer and exhibit a net negative (positive) IEDM.

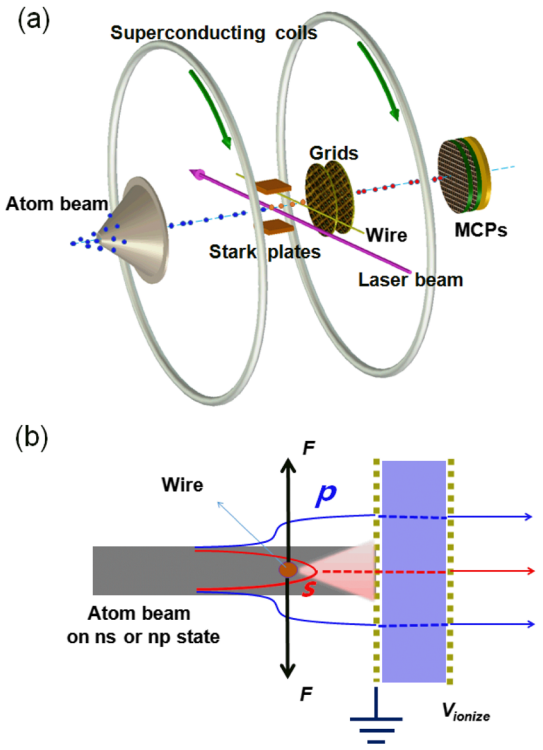

FIG. 3. Experimental setup (a) and atomic trajectory illustrations (b). A weak F field of 20 V/cm between the Stark plates is always present to prepare red $31s$ Rydberg atoms by a suitable resonant one-photon excitation. The copper wire parallel to the laser beam is kept at a nonzero voltage to generate a 2D radial gradient electric field $\vec{\mathbf{F}}$, where the thick black arrows right above and below the wire serve as the F component of the crossed fields. The red state atoms gain more energy in the dashed region along the trajectory due to an earlier ionization in the crossed fields.

We set up a sensitive apparatus as shown in Fig. 3 to falsify the above enhanced LZT scenario for Rydberg atoms prepared on state $31s$. A sodium atomic beam is intersected perpendicularly by a pulsed laser, which prepares the Rydberg states, as in Fig. 3(a). A weak F field of 20 V/cm generated by a pair of parallel Stark plates separated by $d = 1$ cm is always present in the state preparation region, which ensures that the red $31s$ state Rydberg atoms can also be produced by one-photon laser excitation from the ground state $3s$ [30,31].

Immediately after the initial state preparation of $31s$ or $30p$ atoms from photon absorption at their respective resonances, a copper wire parallel to the laser beam is kept at an electric potential V_{wire}, which produces a 2D radial gradient F field [32–36]. A Rydberg atom passing by the wire will be attracted to it or repelled away depending on the sign of its IEDM [34] [see Fig. 3(b)], if a fixed sign dipole moment does exist. The trajectory change occurs mainly in the regions right above and below the wire, where the effect of deflection is maximum. If the resulting force from the IEDM is attractive and sufficiently strong, an atom will be steered into the (pink) region between the wire and the grounded grid placed 2 mm downstream and get ionized. Atomic ions produced this way travel faster after gaining additional kinetic energy from the electric potential difference between the wire and the grid, denoted by the red dashed line, while those deflected away do not (shown by the blue dashed line). Therefore, the implication is that an efficient LZT is transformed and amplified into a faster TOF flight signal.

The fast TOF signal is expected only for those red state Rydberg atoms with large IEDMs, whose net dipole moments are nevertheless nearly zero for sodium in a pure electric field as shown in Fig. 2(a). However, if we apply a magnetic field aligned along the atom beam, this signal becomes observable due to the net IEDM induced by the crossed-field effect as we propose in Fig. 2(b). The radial gradient electric field in the regions right above and below the wire as shown in Fig. 3(b) serves as the F component of the crossed fields, and is denoted by the thick black arrows. The magnetic field is supplied by a superconducting magnet bore (Oxford Instruments), and the ion detector (microchannel plates) is mounted along the central line but is outside of the bore to avoid disturbance from the magnetic field [37,38].

The faster component of the TOF signal is indeed observed experimentally, which confirms that only for the $31s$ state atoms in crossed fields can this occur. Figures 4(a) and 4(b) summarize the observations for the cases in pure magnetic and crossed fields while the TOF spectra are redrawn for the selected red and blue states in Figs. 4(d) and 4(e). A TOF spectrum for an atom in a pure electric field is also shown in Fig. 4(c), which serves as a reference, where atoms prepared in the adiabatic $31s$ or $30p$ states, respectively shown by the black line connected red or blue open circles, are found to carry no net IEDMs. As indicated, their adiabatic passages occur over the avoided level crossings even in the presence of a polarizing F field with the wire voltage set at $V_{\text{wire}} = 170$ V. Their TOF signals remain essentially the same as those shown in Fig. 4(d) for the case of a pure B field with no IEDM. The pair of connected blue open circle traces in Fig. 4(d) denotes the doublet $30p$ feature arising from the paramagnetic interaction, labeled by $30p+$ and $30p-$, respectively [28]. Our observations shown in Figs. 4(c) and 4(d) indicate that the attractive force on the red state atoms alone inside a pure F field is insufficiently strong to deflect the atoms into the early ionization region due to their small net IEDMs from unfavorable LZTs.

However, Fig. 4(e) shows very different TOF traces for atoms in the diabatic $31s$ state when both the crossed F ($V_{\text{wire}} = 170$ V) and B fields ($B = 0.8$ T) are present. Atoms in the $31s$ state now carry negative net IEDMs and are strong field seekers. They are steered towards the copper wire while passing by, which results in their early ionizations within the (pink) wire-grid area. Their corresponding TOF ($t = 17\mu$s) is shorter than the usual value of $t = 21$ μs

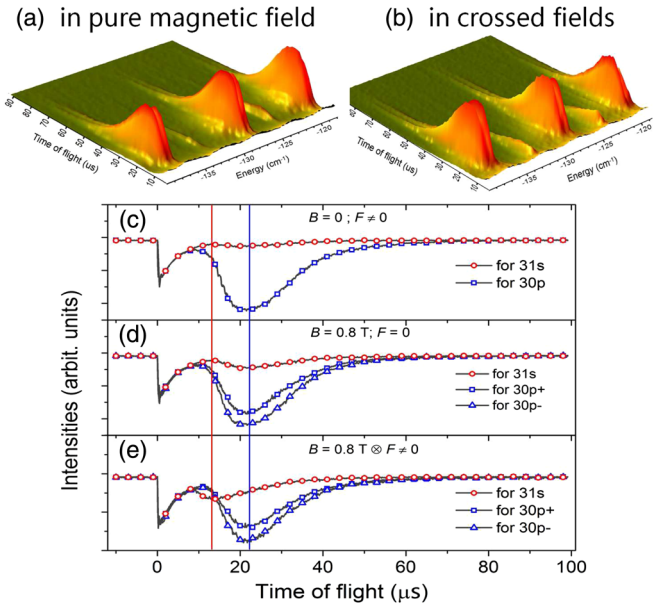

FIG. 4. Observed TOF spectra for Rydberg atoms in a pure B field (a) and in crossed fields (b), where the signal is inverted upside down for better viewing. Specifically, the corresponding TOF signals for $31s$ and $30p$ state atoms are redrawn in (d) and (e), respectively, while the TOF signal for an atom in a pure gradient F field in (c) serves as a reference. Different from that shown in (c) and (d), the atoms in the $31s$ state travel much faster than the $30p$ state ones as shown in (e), implicating their observable kinetic energy gains due to the LZT induced net IEDMs.

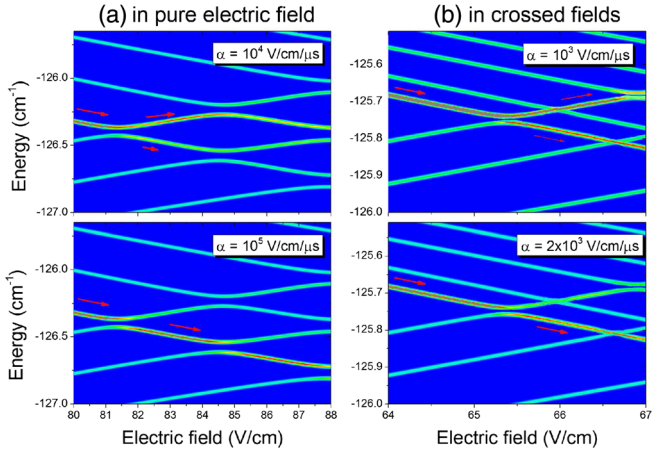

FIG. 5. The dependence of the atomic probability distribution dynamics among the Stark states on the F field sweeping rate for a sodium atom initially prepared in the red state $31s$. In the pure F field (a), a fast rate of $\alpha = 10^5$ V/cm μs is required for a significant LZT. This reduces to $< 2 \times 10^3$ V/cm μs in crossed fields (b), demonstrating that a crossed B field enhances the LZT.

for atoms ionized after passing the first grid as shown in Figs. 4(c) and 4(d). On the contrary, atoms in the diabatic $30p$ state are repelled away from the wire due to their positive signed net IEDMs and are ionized only after the grounded grid, showing a usual flight time of $t = 21$ μs. The sharp inverted dip at $t = 0$ is due to UV pump photons scattered into the detector, which serves to calibrate the beginning of the TOF. The different behaviors for the red state $31s$ in noncrossed fields [Figs. 4(c) and 4(d)] versus in crossed fields [Fig. 4(e)] imply adiabatic versus nonadiabatic behavior while passing over the level crossings, respectively.

Assuming the LZTs occur efficiently for the red $31s$ state atoms and that they indeed carry IEDMs of a fixed sign, we can estimate the typical atomic kinetic motion in the gradient F field surrounding the charged copper wire. We consider as an example a circular orbit trajectory located 1 mm above the copper wire center (of radius $r_w = 0.25$ mm) as shown in Fig. 3(a). According to the Stark map in Fig. 2(b), the diabatic $31s$ state possesses a net IEDM of $\mu_d \sim 1000$ a.u., which corresponds to a dipole interaction potential $U(r) = \mu_d F_r(r) \sim 6$–$13$ meV, with the F field strength estimated according to $F_r(r) = V_{\text{wire}}/\ln(R_0/r_w)/r$, and a length scale parameter $R_0 = 1$–5 mm, depending on the distance to the grid and the Stark plates. This estimation is based on approximately treating the wire's outer radius as a hypothetical hollow metallic cylinder [34]. For an average initial atomic velocity $v \sim 450$ m/s, the corresponding kinetic energy for a sodium atom is around $E_k = mv^2/2 \sim 24$ meV, which is of the same order of magnitude of the electric dipole interaction energy $U(r)$. Atoms getting as close as 1 mm to the wire will thus be steered closer to the wire, eventually arriving at the wire-grid region and getting ionized earlier there. Within such a scheme, the sign of the net IEDM is kept fixed by the diabatic LZTs between successive avoided crossing levels. The analogous switching on or off of the electric field pulse experienced by an atom in its rest frame is extremely fast, on the time scale of the high velocity atoms traversing the wire's inhomogeneous electric field (~ 1 μs), which roughly corresponds to a sweeping rate of close to 10^4 V/cm μs. Nevertheless, it remains much slower than 10^5 V/cm μs as required for a complete LZT in a pure F field [14] as shown in Fig. 5(a). The introduction of the crossed B field reduces the required critical sweeping rate for an efficient LZT down to 2×10^3 V/cm μs, which is supported by detailed numerical simulations as shown in Fig. 5(b). We also find numerically that the LZT rate still retains a value of $\sim 70\%$ at a lower field of $B = 0.6$ T at a fixed sweeping rate (10^4 V/cm μs), which should remain observable experimentally.

In conclusion, we report the experimental observation of an enhanced LZT due to atomic level symmetry breaking. The high LZT rate inside crossed F and B fields helps a Rydberg atom to display a large IEDM of a fixed sign, which causes observable changes to the atomic center of mass motion in a gradient F field. This scenario of symmetry breaking facilitated control of LZTs by Rydberg atoms promises interesting applications to dipole interaction mediated quantum processes [39,40], especially concerning their conditional dynamics such as in a dipole blockade with couplings of a large number of quantum states and pathways [41].

We thank Dr. S. Hogan of University College London, United Kingdom, for helpful discussions. This work is supported by the National Natural Science Foundation of China (Grants No. 91121005, No. 91421305, No. 11674359, and No. 11374176), and by the MOST of the National Key Basic Research Program of China (Grant No. 2013CB922003).

*Corresponding author.
liuhongping@wipm.ac.cn

[1] Y.-A. Chen, S. D. Huber, S. Trotzky, I. Bloch, and E. Altman, Nat. Phys. **7**, 61 (2011).
[2] A. Palii, B. Tsukerblat, J. M. Clemente-Juan, and E. Coronado, J. Phys. Chem. C **116**, 4999 (2012).
[3] M. Sillanpää, T. Lehtinen, A. Paila, Y. Makhlin, and P. Hakonen, Phys. Rev. Lett. **96**, 187002 (2006).
[4] W. D. Oliver, Y. Yu, J. C. Lee, Janice, K. K. Berggren, L. S. Levitov, and T. P. Orlando, Science **310**, 1653 (2005).
[5] S. Gasparinetti, P. Solinas, and J. P. Pekola, Phys. Rev. Lett. **107**, 207002 (2011).
[6] M. F. Gonzalez-Zalba, S. N. Shevchenko, S. Barraud, J. R. Johansson, A. J. Ferguson, F. Nori, and A. C. Betz, Nano Lett. **16**, 1614 (2016).
[7] G. Cao, H. O. Li, T. Tu, L. Wang, C. Zhou, M. Xiao, G. C. Guo, H. W. Jiang, and G. P. Guo, Nat. Commun. **4**, 1401 (2013).
[8] G. Sun, X. Wen, B. Mao, J. Chen, Y. Yu, P. Wu, and S. Han, Nat. Commun. **1**, 51 (2010).
[9] M. Gong, X. Wen, G. Sun, D. W. Zhang, D. Lan, Y. Zhou, Y. Fan, Y. Liu, X. Tan, H. Yu, Y. Yu, S. L. Zhu, S. Han, and P. Wu, Sci. Rep. **6**, 22667 (2016).
[10] J. R. Petta, H. Lu, and A. C. Gossard, Science **327**, 669 (2010).
[11] C. Betthausen, T. Dollinger, H. Saarikoski, V. Kolkovsky, G. Karczewski, T. Wojtowicz, K. Richter, and D. Weiss, Science **337**, 324 (2012).
[12] M. D. LaHaye, J. Suh, P. M. Echternach, K. C. Schwab, and M. L. Roukes, Nature (London) **459**, 960 (2009).
[13] C. Zener, Proc. R. Soc. A **137**, 696 (1932).
[14] M. Førre and J. P. Hansen, Phys. Rev. A **67**, 053402 (2003).
[15] T. F. Gallagher, *Rydberg Atoms* (Cambridge University Press, Cambridge, England, 1994).
[16] R. Feynman, J. Hollingsworth, M. Vennettilli, T. Budner, R. Zmiewski, D. P. Fahey, T. J. Carroll, and M. W. Noel, Phys. Rev. A **92**, 043412 (2015).
[17] M. L. Zimmerman, M. G. Littman, M. M. Kash, and D. Kleppner, Phys. Rev. A **20**, 2251 (1979).
[18] R. R. Jones and T. F. Gallagher, Phys. Rev. A **39**, 4583 (1989).
[19] A. S. Stodolna, F. Lepine, T. Bergeman, F. Robicheaux, A. Gijsbertsen, J. H. Jungmann, C. Bordas, and M. J. J. Vrakking, Phys. Rev. Lett. **113**, 103002 (2014).
[20] J. R. Rubbmark, M. M. Kash, M. G. Littman, and D. Kleppner, Phys. Rev. A **23**, 3107 (1981).
[21] A. Gürtler and W. J. Van Der Zande, Phys. Lett. A **324**, 315 (2004).
[22] F. Merkt, R. J. Rednall, S. R. Mackenzie, and T. P. Softley, Phys. Rev. Lett. **76**, 3526 (1996).
[23] See Supplemental Material at http://link.aps.org/supplemental/10.1103/PhysRevLett.120.063203 for the detailed description of energy level calculation.
[24] H. Bachau, E. Cormier, P. Decleva, J. E. Hansen, and F. Martin, Rep. Prog. Phys. **64**, 1815 (2001).
[25] F. Robicheaux, C. Wesdorp, and L. D. Noordam, Phys. Rev. A **62**, 043404 (2000).
[26] X. M. Tong and S.-I. Chu, Phys. Rev. A **61**, 031401 (2000).
[27] G. Wiebusch, J. Main, K. Krüger, H. Rottke, A. Holle, and K. H. Welge, Phys. Rev. Lett. **62**, 2821 (1989).
[28] O. Tkáč, M. Žeško, J. A. Agner, H. Schmutz, and F. Merkt, J. Phys. B **49**, 104002 (2016).
[29] G. M. Wysin, Associated legendre functions and dipole transition matrix elements, https://www.phys.ksu.edu/personal/wysin/.
[30] M. H. Halley, D. Delande, and K. T. Taylor, J. Phys. B **26**, 1775 (1993).
[31] I. Seipp and K. T. Taylor, J. Phys. B **27**, 2785 (1994).
[32] J. Schmiedmayer, Appl. Phys. B **60**, 169 (1995).
[33] R. Barnett, D. Petrov, M. Lukin, and E. Demler, Phys. Rev. Lett. **96**, 190401 (2006).
[34] H. Ko and S. D. Hogan, Phys. Rev. A **89**, 053410 (2014).
[35] S. K. Sekatskii and J. Schmiedmayer, Europhys. Lett. **36**, 407 (1996).
[36] H. J. Loesch, Chem. Phys. **207**, 427 (1996).
[37] W. Gao, H. F. Yang, H. Cheng, X. J. Liu, and H. P. Liu, Phys. Rev. A **86**, 012517 (2012).
[38] H. F. Yang, W. Gao, W. Quan, X. J. Liu, and H. P. Liu, Phys. Rev. A **85**, 032508 (2012).
[39] M. Saffman, T. G. Walker, and K. Molmer, Rev. Mod. Phys. **82**, 2313 (2010).
[40] M. D. Lukin, M. Fleischhauer, R. Cote, L. M. Duan, D. Jaksch, J. I. Cirac, and P. Zoller, Phys. Rev. Lett. **87**, 037901 (2001).
[41] S. R. de Echaniz, A. D. Greentree, A. V. Durrant, D. M. Segal, J. P. Marangos, and J. A. Vaccaro, Phys. Rev. A **64**, 013812 (2001).